Fluid Force-Induced Detachment Criteria for Nonmetallic Inclusions Adhered to a Refractory/Molten Steel Interface

UXIA DIEGUEZ SALGADO, CHRISTIAN WEIß, SUSANNE K. MICHELIC, and CHRISTIAN BERNHARD

Since nonmetallic inclusions (NMIs) in steel cannot be completely avoided, a greater understanding of their development and evolution during the steelmaking process is required. In particular, this includes the adhesion of microinclusions to the refractory/steel interface in the flow control system between the tundish and the mold. This phenomenon, commonly referred to as clogging, causes losses in productivity and product quality. Inclusions transported from the bulk melt to the boundary layer may adhere to the refractory/steel interface due to formation of a fluid cavity. A detailed model was derived for the detachment of NMIs adhering to a nozzle wall and is based on the local hydrodynamic conditions combined with the specific interfacial properties in the system consisting of the inclusions, the refractories, and the steel. The model is evaluated for three different application-oriented cases. This study has been focused on providing a better understanding of fluid flow in the near-wall region in order to reduce clogging during steelmaking.

https://doi.org/10.1007/s11663-018-1271-2
© The Minerals, Metals & Materials Society and ASM International 2018

I. INTRODUCTION

NONMETALLIC inclusions (NMIs) in steel have a considerable impact on the final product quality with regard to properties such as dynamic loads, corrosion resistance, and optical appearance. An excessive number of microinclusions or inclusions with an unsuitable morphology can also lead to problems in the processing of steel, such as clogging, during the continuous casting process or breakage during cold drawing.[1] Since inclusions cannot be completely avoided, a greater understanding of the formation, development, and evolution of inclusions through each processing step of steel manufacturing is necessary. The present article mainly focuses on the behavior of small oxidic inclusions with a diameter below 10 μm in the fluid flow control system of a continuous caster.

These micro-oxide inclusions mostly result from the deoxidation of the steel and the subsequent interaction with ladle slag and ladle lining.[1,2] Initially, very small particles collide and agglomerate in liquid steel to form larger particles. Ladle stirring is the most common method to stimulate the agglomeration and flotation of particles and finally to separate the particles into the slag. Nevertheless, a large number of microparticles stay suspended in the liquid steel and pass onto the next processing stage, the casting process.[1–3] Over the entire process, interfacial phenomena significantly influence nucleation, agglomeration, flotation, or separation of the particles.[3]

NMIs may, depending on their composition, size, and morphology, become troublesome in the fluid flow control system of a caster tundish, namely, in the submerged entry nozzle (SEN). The SEN, which is presented schematically in Figure 1(a), is a pipelike refractory component placed between the tundish and the mold in a continuous caster. It prevents the steel from oxygen and nitrogen pickup and ensures a stable casting operation in the mold.[1] The adhesion of oxide particles at the SEN surface is one of the commonly recognized initial stages for the development of clogs. This results in an uneven reduction of the inner diameter of the nozzle; consequently, the caster operation may be seriously disrupted, possibly diminishing the slab surface and subsurface quality.[2] The phenomenon described previously is known as clogging,[1–6] and these deposits are found along the SEN as well as in areas of the stopper rod, as shown in Figure 1(b).

UXIA DIEGUEZ SALGADO, SUSANNE K. MICHELIC, and CHRISTIAN BERNHARD are with the Department of Ferrous Metallurgy, the Montanuniversitaet Leoben, Leoben, 8700, Austria. Contact email: Uxia.Dieguez-Salgado@unileoben.ac.at CHRISTIAN WEIß is with the Department of Environmental and Energy Process Engineering, the Montanuniversitaet Leoben, Leoben, 8700, Austria.
Manuscript submitted November 13, 2017.
Article published online May 8, 2018.

Numerous studies have been carried out in order to elucidate the clogging mechanism for deposits at the nozzle in continuous casting. Rackers and Thomas,[2] Singh,[5] and Thomas and Bai[8] summarized the clogging of the SEN as four mechanisms:

(i) agglomeration of deoxidation products at the steel/refractory interface due to fluid flow and interfacial tension effects;[4–6,9–11]
(ii) air aspiration into the nozzle and subsequent reoxidation of the steel at the steel/refractory interface[12–17] (the aspirated oxygen may create a surface tension gradient in the steel near the wall and, therefore, increase the attractive force toward the wall);
(iii) chemical reactions between the nozzle refractory and the steel[12,18–29] (this type of clogging is attributed to reactions between diffused oxygen coming from the refractory and aluminum from the steel); and
(iv) solid steel buildup during the start of casting when the preheating of the nozzle is inadequate or within a clog matrix where the flow rate is very slow.[15,23,30–33]

Nevertheless, a given nozzle deposit is often the result of more than one of the aforementioned mechanisms. The present article focuses on the clogging caused by agglomeration of small deoxidation products at the SEN wall.

Generally, two spherical inclusions approaching each other in the molten steel will tend to agglomerate to form larger particles due to interfacial contact forces. The same behavior is expected for inclusions approaching a nozzle wall.[34] The deposition process of NMIs at a steel/refractory interface is described schematically in Figure 2.[4,5] A similar mechanism is also applicable to particle deposition in steel filtration by a ceramic filter.[35–37]

(i) Transport: the NMIs that are transported from the bulk region to the boundary layer eventually may come in contact with the nozzle refractory.
(ii) Adhesion: the inclusions adhere to the refractory wall by interfacial forces, eventually leading to a fluid cavity formation around the contact point.
(iii) Sintering: due to the high temperatures involved, the inclusions sinter at the wall, forming a solid structure.

Table I summarized some of the research done in the field of NMI deposition at a steel/refractory interface. Although there exists common agreement on the deposition of NMIs as an empirical fact, debate considering transport and the sticking mechanism by which inclusions are enabled to adhere at the wall still remains unsettled.

The NMIs that are transported from the bulk region to the boundary layer eventually may come in contact with the nozzle refractory. In general, there are two theories regarding the transport of NMIs toward a wall.

(1) The boundary layer theory proposed by Singh:[5] He suggests that the speed of the inclusions slows when they enter the boundary layer, where the velocity of the stream approaches zero. The particles, especially the ones closest to the surface, have a very low relative velocity against the wall and will adhere to the refractory wall in order to reduce the interfacial

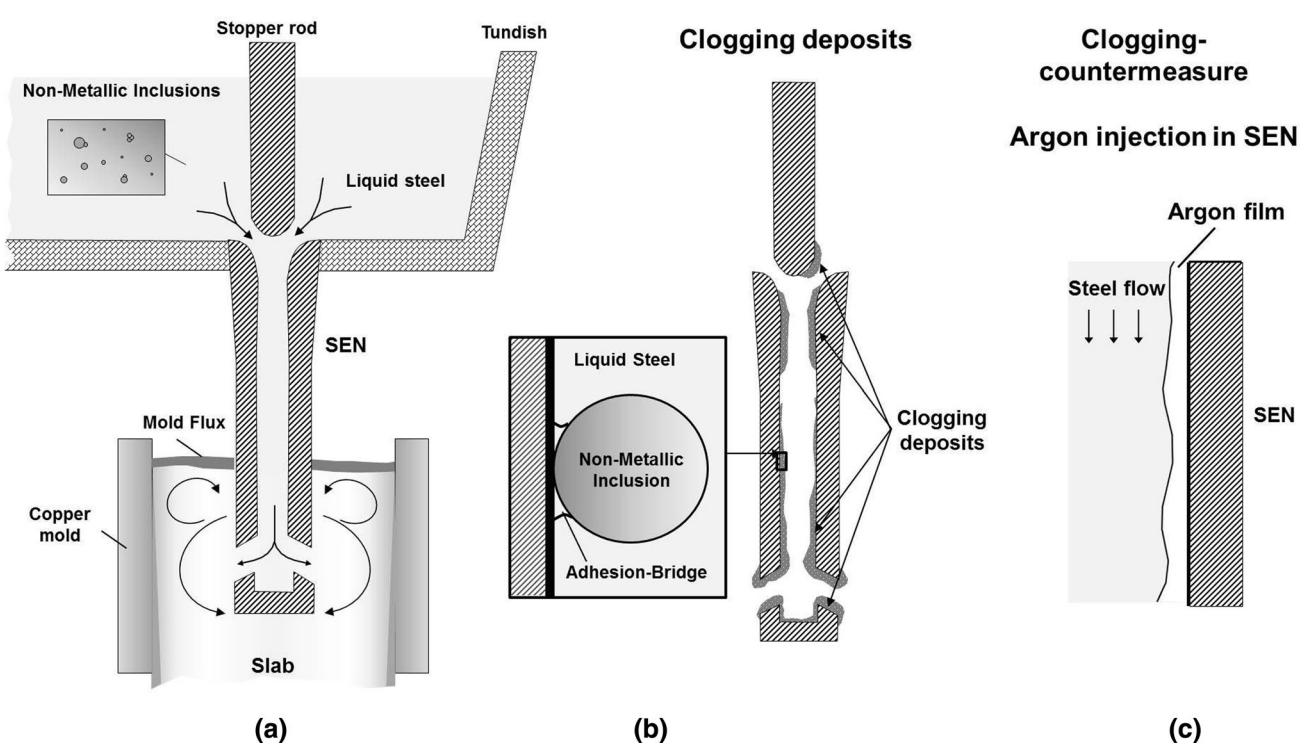

Fig. 1—(*a*) Schematic representation of the SEN connecting the tundish and the copper mold, (*b*) position of the clogging deposits, and (*c*) clogging countermeasure by Ar injection. (The last one is adapted from Ref. [7]).

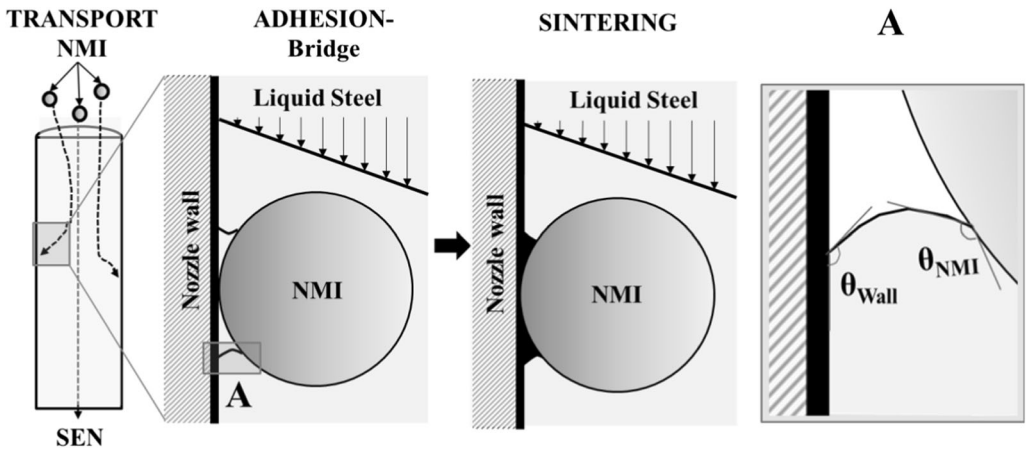

Fig. 2—Deposition process of NMIs transported from the bulk flow region into the boundary layer at the steel/refractory interface: transport, adhesion, and sintering. Detail A represents the cavity contour, which is determined by the contact angle between the nozzle wall and the steel, $\theta_{Wall} = \theta_2$, and the contact angle between the NMI and the steel, $\theta_{NMI} = \theta_1$.

Table I. Summary of the Research Done about NMI Deposition at a Steel/Refractory Interface

	Deposition Steps			
References	T	A	S	Details
Singh[5]	X			general description of the steps; boundary layer theory
Wilson *et al.*[4]	X			local eddy transport phenomena
Dawson[15]	X			local eddy transport phenomena
Uemura *et al.*[35]		X	X	filtration of NMI in steel at a ceramic loop filter
Sasai and Mizukami[34] and Sasai[38]		X	X	Al_2O_3 adhesion at a continuous caster nozzle
Kawecka-Cebula *et al.*[36]		X		filtration of NMI in molten steel
Mizoguchi and co-workers[39,40]		X		influence of iron oxide in adhesion force
Zheng *et al.*[41,42]		X		effect of NMI morphology in adhesion force
Xuan *et al.*[43]		X	X	Al_2O_3 particle agglomeration in the melt

T transport, *A* adhesion, *S* sintering.

energy of the system.[5,6,20,44] This theory agrees with the conclusions given by Wilson *et al.*[4] and Dawson[15] that suggest that recirculation and dead zones are areas of high deposition tendency.

(2) The local eddy transport phenomena proposed as a summary of the research performed by Wilson *et al.*[4] and Dawson,[15] among others: This approach suggests that turbulence conditions can strongly increase the deposition of the inclusions.

The attachment results in the spontaneous formation of fluid bridges between the inclusion and the wall, as shown in Figure 2.[34–36,38–43] The conditions become favorable for particle adhesion when

$$\sigma_{pr}\Delta S_{pr} < \sigma_{pm}\Delta S_{pm} + \sigma_{mr}\Delta S_{mr} \quad [1]$$

where σ = surface tension, ΔS = change in surface energy, p = particle, r = refractory, and m = metal. The work of adhesion is given by

$$W = \sigma_{pm}(1 - \cos\theta) \quad [2]$$

where θ is the contact angle.[4,5]

The contact angle of NMIs is found to be nonwetting in most cases; *i.e.*, the contact angle of Al_2O_3 in steel is estimated to be 137 deg in liquid iron.[4,5,45] When the contact angle of an inclusion within molten steel is at a maximum, the adherence between the inclusions and the refractory will be at a maximum. Since the contact angle of alumina in steel is high, whenever alumina particles come in contact with a similar surface (such as another alumina particle or any refractory surface), they will attach to each other in order to minimize the surface energy.[4,5] Because of the high temperatures involved, sintering will start immediately following primary contact. Further inclusions collide and attach to each other, forming a strong network that continuously reduces the inner diameter of the SEN.[5]

A certain number of techniques have been developed in order to decrease the deposition of small oxides at the nozzle wall, such as the following.

(i) Use of alternative nozzle materials[6,46,47] such as lime-bearing refractories,[28,46,48–51] calcium zirconate refractories,[48,50,52] calcium titanate materials,[28] O'-SiAlON-ZrO_2 materials,[53] and

BN-enriched materials:[47] The new materials are selected for their ability to form low melting compounds as a result of the reaction between the refractory and the solid alumina particles from the steel. These low melting point inclusions most likely will be washed away from the wall.

(ii) Development of new nozzle designs for a better control of the steel flow: Some examples are annular step nozzles,[54] nozzles with heat insulation,[55] bubble curtain nozzles,[56] and several others.[57]

(iii) Improvement of the deoxidation practice by converting deoxidation products to low melting point–type inclusions by calcium treatment of the steel:[4,6,58–64] The calcium reacts with aluminum in the steel, forming liquid calcium aluminates, which are less likely to form agglomerates.

(iv) Argon injection in the SEN[2,6,7,16,17,65] to reduce possible contact between inclusions and the nozzle wall and to promote the removal of inclusions by flotation: In their water model experiments, Thomas *et al.*[7] observed that at large Ar injection rates and high water flow, the argon bubbles elongate along the wall, forming a gas layer. A representation on how the argon layer at the SEN wall may look is shown in Figure 1(c). This layer prevents the physical contact between the steel stream and the refractory wall and, thus, prevents the buildup of inclusions on the SEN wall.

Even if argon injection is commonly applied in industrial practice as a clogging countermeasure, it is still unclear which hydrodynamic conditions favor the attachment or detachment of the NMIs at the nozzle wall. To resolve some of these issues, the current work proposes a detailed micromechanical model for the detachment of NMIs adhering to a nozzle wall, based on the hydrodynamic conditions present in the wall boundary layer. The model is evaluated for different material properties such as surface tension and contact angle. No discussion of the transport or the sintering steps will be given.

II. MODEL DESCRIPTION

A single spherical micro-oxide adheres by forming a cavity bridge against the nozzle wall, as illustrated in Figure 2. This inclusion will be subjected as well to detachment forces related to the material properties and to the fluid flow conditions in the near-wall region. A detachment criterion is presented based on the normal and parallel force balances and on the torque moment of the inclusion. The model comprises the following assumptions and simplifications.

1. The source of the clogging deposit comes from the agglomeration of small oxidic inclusions at the nozzle wall. From the three-step mechanism defined in Figure 2, only the adhesion step is considered here.
2. The small inclusions with a spherical shape are attached to the wall by a fluid cavity. The source of the cavity is already present in the system, meaning that no argon injection is considered for the analysis.
3. The nozzle wall is assumed to be flat and smooth.

A. *Attractive Forces*

If a spherical inclusion approaches a nozzle wall, the steel in the contact area withdraws, leaving a cavity, as represented in Figure 3.[34–36,38] The adhesion of particles in terms of capillary or cavity forces is a direct consequence of the surface contour of the bridge-fluid phase,[66,67] and it is attributed to the fact that steel is unlikely to wet solid NMIs. The cavity might be filled with (i) gaseous components originally dissolved in the melt, (ii) gaseous components coming from the refractory, (iii) melt vapor, or (iv) liquid phases forming due to a local rise in the oxygen concentration.

Fisher[68] expressed the adhesion force in terms of a cavity formation, considering (i) the tension exerted by the steel-fluid interface and (ii) the resultant force when the cavity pressure is lower than in the steel. Two methods are established for the calculation of adhesion forces, and they differ in the point at which the forces are applied.[66,67,69,70] For the boundary method, the force is calculated on the contact line between solid, liquid, and gas, whereas the force is calculated at the thinnest point of the cavity for the neck method. Both methods show reasonable accuracy theoretically, experimentally, and numerically.[71] If R_2 is the radius of the neck of fluid connecting the two bodies, the tension exerted by the interface at the neck is $2\pi R_2\sigma$ and the tensile force due to the pressure difference is $\pi R_2^2\Delta P$. The force balance calculated at the thinnest point of the neck is written as follows:

$$F_A = 2\pi R_2\sigma + \pi R_2^2\Delta P \quad [3]$$

where σ is the surface tension of molten steel and ΔP is the pressure difference between the steel and the cavity phases.[34–36,38,39,41,72]

The cavity geometry is determined based on the toroidal approximation, which assumes a constant curvature of the contour[66,67]:

$$\begin{aligned} &-2r_1r_2[R_1(\cos\theta_1+\cos\theta_2)+d] \\ &-(r_1+r_2)\left(\frac{d^2}{4}+2R_1R_2'+R_2'^2\right) \\ &-d\left(R_1+R_2'\right)(r_1-r_2)\cdot\cos\alpha=0 \end{aligned} \quad [4]$$

$$\cos\alpha = \frac{R_1(r_2\cos\theta_2 - r_1\cos\theta_1) - d(r_1-r_2)}{-(R_1+R_2)(r_1+r_2+d)} \quad [5]$$

$$R_2 = R_2'\cdot\sin\alpha \quad [6]$$

where r_1 and r_2 are the inclusion and the refractory radii, respectively; θ_1 and θ_2 are the contact angle between the inclusion and the molten steel and the wall and the molten steel, respectively; R_1 and R_2 are the cavity radii; α is an auxiliary angle; R_2' is an auxiliary radius; and d is the particle distance from the wall. Geometrical details of these parameters are given in Figure 3.

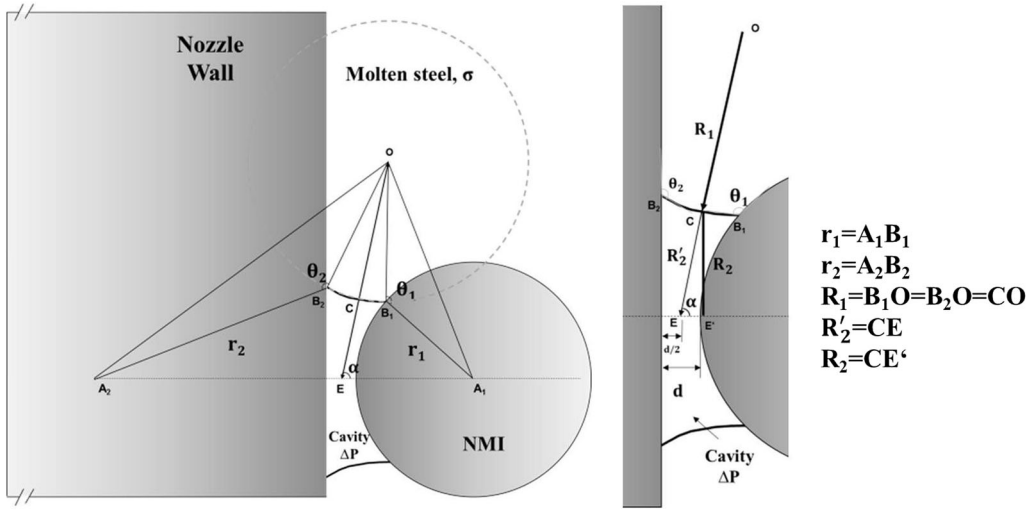

Fig. 3—Attraction force between an NMI and a nozzle wall by bridge formation for particle distance $d << r_1$.

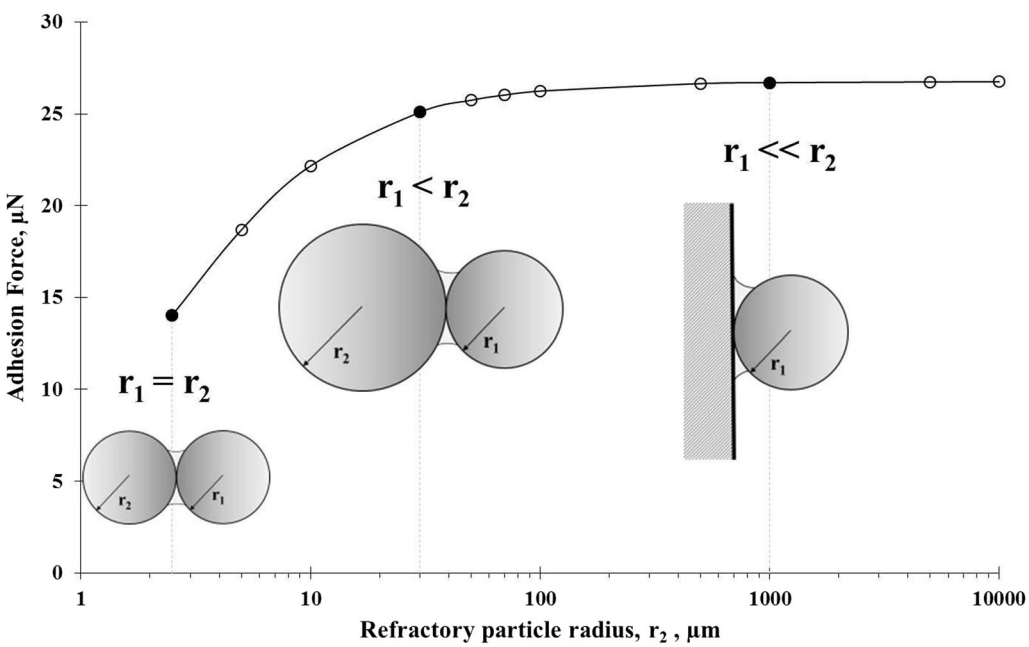

Fig. 4—Influence of the size of the second particle, r_2, on the adhesion force.

The mechanical equilibrium of the bridge interface is given by the Young–Laplace equation, which relates the pressure difference across the interface to both the mean curvature of the interface and the interfacial tension between the contacting fluids[67,69,73]:

$$\Delta P = \sigma \cdot \left(\frac{1}{R_1} - \frac{1}{R_2} \right) \qquad [7]$$

The Young–Laplace equation is required for calculating the adhesion force. However, both the mean curvature and the pressure difference across the steel/cavity interface are not directly known due to the lack of *in-situ* observations. On one hand, a way to confront this issue is to define the volume of the cavity. For that purpose, postmortem analysis of extracted agglomerated inclusions may be necessary. This kind of analysis may not provide accurate data due to shrinkage of the cavity during cooling. Alternatively, the calculation of the pressure across the bridge may offer a more direct approach. Assuming a lower pressure inside the cavity (vapor pressure of iron = 7.6 Pa), the molten steel pressure will be defined as the atmospheric pressure plus the local ferrostatic pressure. A pressure difference of $1.8 \cdot 10^5$ Pa at 1-m depth[34] was chosen as a rough estimate for the current work.

The bridge force between two particles reaches a more or less constant value when increasing the size of one particle, keeping the second one at a constant size. To explore this configuration in detail, we consider the adhesion force between two spherical particles approaching each other. Assume that the first particle

has a 2.5-μm radius (r_1) and is a NMI formed due to steel deoxidation and assume the second particle (r_2) originates from the refractory material. Both particles are aluminum oxides with a corresponding contact angle of 137 deg with the molten steel. In Figure 4, the influence of the size of the second particle on the adhesion force is shown as a function of r_2 at a melt depth of 1 m and 1.8 N/m of molten steel surface tension, and this curve was plotted by solving Eqs. [3] through [7]. When the size of the refractory particle (r_2) is increased, the force rises until it reaches a constant value when the diameter is greater than approximately 50 μm. In other words, if the refractory particle is much bigger than the NMI ($r_1 \ll r_2$), the adhesion force between a NMI and a refractory wall can be calculated explicitly. This approach will be used for the rest of the adhesion force calculations in this work.

Considered is the van der Waals force, which is always present at distances from several nanometers to the size of the interatomic spacings. When the interparticle distance is smaller than the inclusion size, the van der Waals force acting between two spherical inclusions of different sizes is given by Eq. [8]:

$$F_{\mathrm{vdW}} = A_H \frac{1}{6d^2} \cdot \frac{r_1 r_2}{r_1 + r_2} \forall\, d \ll r_1 \qquad [8]$$

where r_i is the radius of the spherical particle (i = 1, 2) (m), d is the interparticle distance (m), and $A_{\mathrm{H}} = 1.45 \cdot 10^{-18}$ J is the Hamaker constant.[34,74] The Hamaker constant depends on the material properties and the steel temperature, and the value was corrected by Xuan *et al.*[43]

Van der Waals forces greatly change with the interparticle distance and the particle size. If the radius of the second particle is much larger than the first particle ($r_1 \ll r_2$),[74] the van der Waals force will be given by Eq. [9]:

$$F_{\mathrm{vdW}} = -A_H \cdot \frac{r_1}{6d^2} \forall\, d \ll r_1 \qquad [9]$$

Although the exact distance of the bridge formation is unknown due to the difficulties of *in-situ* observation of molten steel, the results of calculations in Figure 5 barely show any change in the adhesion force at small distances. At intermolecular distances, the van der Waals forces will be significant and will rapidly increase with a decrease in distance between the molecules. Note the regime discrimination between the molecular and the continuum capillary forces at a cut-off distance of roughly 10 nm, in accordance with the mean free path of the molecules. Additionally, it should be mentioned that both forces increase with the inclusion size.

Since the relevant particle wall distances due to the cavity bridges clearly exceed molecular ranges, van der Waals forces will not be considered in the remainder of this analysis.

B. *Detachment Forces*

An NMI adhered by a fluid cavity to a refractory may be detached by several force contributions. Buoyancy, drag, and lift forces are considered in the following analysis as possible sources for detachment of the inclusion. Figure 6 represents the forces considered in the system. To simplify the analysis, it will be assumed that the main motion of a particle in the liquid steel is dominated by translation; rotational or swirling motion of the particle in the near-wall region, therefore, will be neglected.

Each NMI submerged in molten steel experiences an upward force opposing its weight, known as buoyancy force, F_B. The buoyancy force depends on the density difference between the inclusion and the steel, the gravity acceleration, and the volume of the submerged inclusion, and is given by the following equation:

$$F_B = \frac{\pi}{6} d_1^3 (\rho - \rho_i) g \qquad [10]$$

where d_1 is the inclusion diameter (m); ρ and ρ_i are the density (kg/m^3) of the molten steel and the inclusion, respectively; and g is the gravity acceleration (m/s^2).

The behavior of adhered NMIs may be influenced as well by the fluid flow in the near-wall region. The flow profile in a circular SEN is characterized by the dimensionless Reynolds number, shown in Eq. [11], and it depends on the ratio of the inertial forces to viscous forces in the fluid.

$$Re = \frac{\text{Inertial forces}}{\text{Viscous forces}} = \frac{u_{\mathrm{avg}} \Phi_{\mathrm{SEN}}}{\upsilon} = \begin{cases} Re \le 2300 \rightarrow & \text{Laminar flow} \\ 2300 \le Re \le 4000 \rightarrow & \text{Transitional flow} \\ Re \ge 4000 \rightarrow & \text{Turbulent flow} \end{cases} \qquad [11]$$

where u_{avg} is the average flow velocity (m/s), Φ_{SEN} is the SEN diameter (m), and υ is the kinematic viscosity of the steel (m^2/s). The laminar flow can be maintained eventually at much higher Reynolds number (up to 10,000) in very smooth pipes.

In a fully developed laminar flow, the velocity profile remains unchanged in the flow direction. The velocity profile represented in Figure 7 is parabolic, with a maximum at the centerline and minimum (zero) at the wall. The profile is of the general form

$$u(x) = 2u_{\mathrm{avg}} \left(1 - \frac{x^2}{(2\Phi_{\mathrm{SEN}})^2} \right) \qquad [12]$$

where x is the radial distance from the centerline of the SEN and u_{avg} is the average velocity in the flow cross section, roughly corresponding to one-half of the maximum velocity.

The turbulent flow along a wall as often encountered in practice is described by four regions that are a function of their distance from the wall: laminar layer, buffer layer, transition layer, and turbulent layer. The laminar layer plays a dominant role in flow characteristics due to the large velocity gradient that occurs. The velocity profile for turbulent flow is quite flat compared to the laminar profile (Figure 7), with a sharp drop near the nozzle wall.

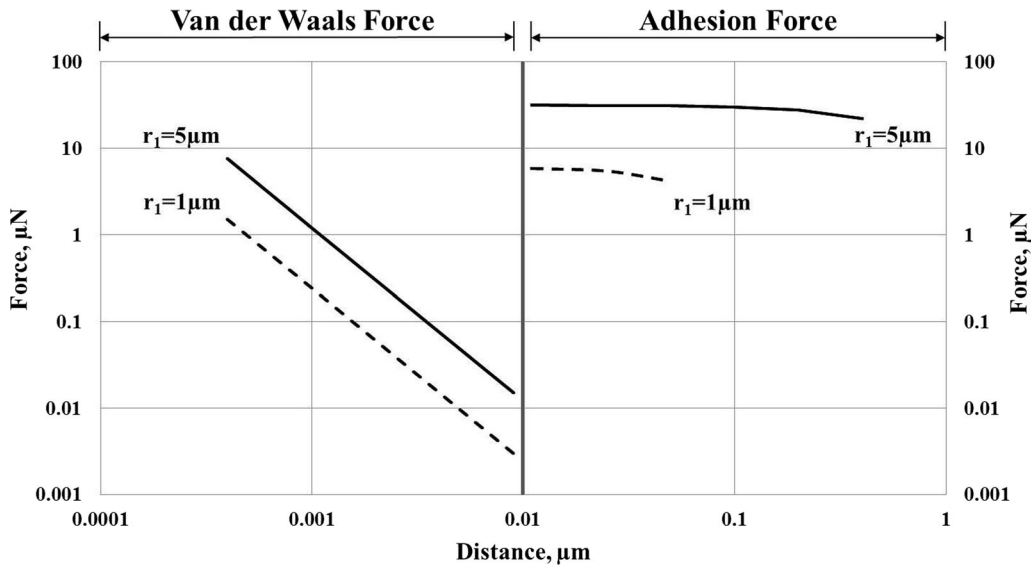

Fig. 5—Van der Waals and adhesion as attractive force contributions and their specific range in terms of interparticle distance.

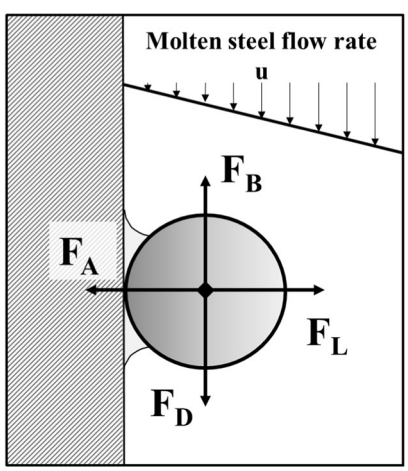

Fig. 6—Forces analyzed on an NMI in contact with a nozzle wall in the boundary layer.

The velocity profile in the laminar layer in dimensionless form is known as "the law of the wall for smooth surfaces" and is shown in Eq. [13]:

$$\frac{u}{u^*} = \frac{yu^*}{\upsilon} \forall 0 \leq \frac{yu^*}{\upsilon} \leq 5 \qquad [13]$$

$$u^* = \sqrt{\frac{\tau_w}{\rho}} \qquad [14]$$

$$\tau_w = \mu \cdot \dot{u} = (\rho\upsilon) \cdot \dot{u} \forall \dot{u} = \frac{du}{dy} \qquad [15]$$

where u^* is the friction velocity (m/s), τ_w is the shear stress (kg/ms^2), μ is the dynamic viscosity of steel (kg/ms), υ is the kinematic viscosity of steel (m^2/s), $\dot{u}$ represents the velocity gradient in the laminar layer (s^{-1}), and y is the distance from the wall (m).

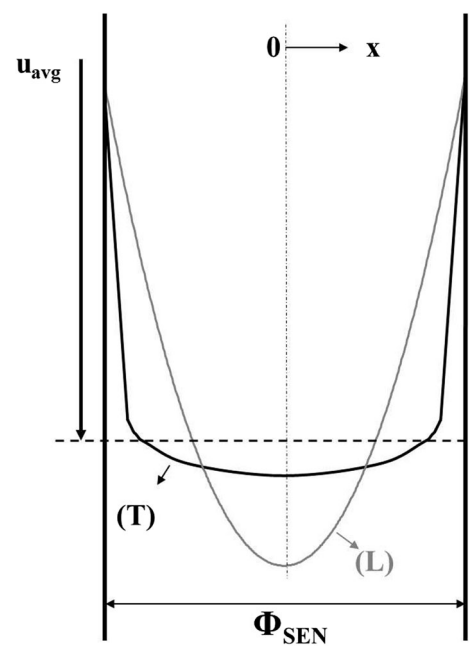

Fig. 7—Velocity profile for a laminar flow (L) and a turbulent flow (T) in a nozzle.

From Eq. [16], the thickness of the laminar sublayer, δ, is calculated and is proportional to the kinematic viscosity and inversely proportional to the friction velocity, as defined previously:

$$\delta = \frac{5\upsilon}{u^*} \qquad [16]$$

In Table II, the flow characteristics of a 30-mm-diameter SEN nozzle are presented. The Reynolds number indicates the presence of a turbulent regime inside the pipe for both velocities considered. The increase of the steel flow velocity in the pipe from 1 to 2 m/s causes a decrease of nearly 100 μm in the thickness of the

Table II. Calculated SEN Characteristics for a 30-mm-Diameter Nozzle

Φ_{SEN} (mm)	u_{max} (m/s)	Re	δ (μm)	u_δ (m/s)
30	1	21,000	~ 370	0.05
	2	42,000	~ 260	0.07

laminar layer. Thus, the laminar layer becomes thinner when the velocity is increased. In addition, the velocity in the laminar layer, u_δ, is in the range of 0.05 to 0.07 m/s at the limit of the boundary layer and zero next to the wall.

Force contributions exerted on an adhered particle in the near region of a nozzle wall are analyzed as follows. A spherical inclusion adhered to the nozzle experiences a drag force due to the relative movement of molten steel. The drag force, F_D, depends on the inclusion surface and on the molten steel properties, such as velocity and density according to Eq. [17][34,38,73]:

$$F_D = C_D \frac{\rho u_r^2}{2} A_1 \qquad [17]$$

where C_D is the drag coefficient; A_1 is the projected area of the inclusion toward the flow direction, defined as $\pi d_1^2/4$ (m^2); and u_r is the relative velocity between the inclusion and the molten steel at the inclusion's mass center (m/s). The drag coefficient on a sphere in steady motion can be estimated by using the empirical correlation proposed by Lapple, given in Eq. [18].[34,38,75] This equation is an interpolation between the Stokes and the Newton regimes in order to cover the range of cases that will be presented in Section III:

$$C_D = \frac{24 \cdot \left(1 + 0.15 \cdot \mathrm{Re}_p^{2/3}\right)}{\mathrm{Re}_p} \forall \quad \mathrm{Re}_p = \frac{u_r d_1}{\upsilon} \leq 1000 \qquad [18]$$

Due to the small particle sizes involved, the particle Reynolds number, Re_p, will be quite small. Thus, the nonstationary drag force terms, such as virtual mass force and Basset force, are not important and, therefore, will not be considered.

In addition to the drag force, the flow passing around the adhered inclusion may create a difference in pressure, resulting in a lifting force normal to the wall.[76,77] Leighton and Acrivos[78,79] defined an expression for the lift force acting on a sphere resting on a wall, F_L, according to Eq. [19]:

$$F_L = 9.22 Re_G \left(\dot{u}\mu r_1^2\right) \forall Re_G = \frac{\dot{u} r_1^2}{\upsilon} \qquad [19]$$

where Re_G is the shear Reynolds number.

C. *Detachment Criteria*

Based on the force contributions already introduced (Figure 6), three criteria in terms of force and torque balances determine whether an inclusion in contact with the wall will be able to be detached from the wall.

1. *Normal movement*

For a detachment of the inclusion particle from the wall in the normal direction, according to the force balance

$$F_A = F_L \qquad [20]$$

the lift force must overcome the adhesion force. In other words, the inclusion will be lifted off if the normal ratio (R_N) is greater than unity, as shown in the equation

$$R_N = \frac{F_L}{F_A} \qquad [21]$$

Since the lift force is directly dependent on the fluid flow conditions next to the wall, any increase in velocity at the near-wall region will increase the normal ratio.

2. *Parallel movement*

In Eq. [22], the parallel movement of the inclusion is analyzed. For that to happen, the resultant tangential force should overcome the friction between the surfaces. The frictional force, F_F, is proportional to the normal force exerted by each surface on the other, directed perpendicular to the surface.

$$(F_D - F_B) = F_F = \kappa_S \cdot F_n = \kappa_S \cdot (F_A - F_L) \qquad [22]$$

$$\mathrm{R}_P = \frac{(F_D - F_B)}{\kappa_S (F_A - \mathrm{F}_L)} \qquad [23]$$

where F_n is the normal force (N), κ_s is the coefficient of friction (chosen to be 0.3 for cases (1) and (2) and 0.1 for case (3) in Section III), and R_p is the parallel ratio. The criterion indicates that the particle will be detached when the parallel ratio is greater than unity. The possibility of a liquid phase acting as a bridge might reduce the dry frictional force, increasing the parallel ratio.

3. *Torque moment*

The torque moment defines the tendency of a force to rotate an object about an axis.[80] Drag and lift forces exerted on the inclusion might induce a torque on the particle:

$$aF_A = 1.4 r_1 F_D + aF_L - r_1 F_B \qquad [24]$$

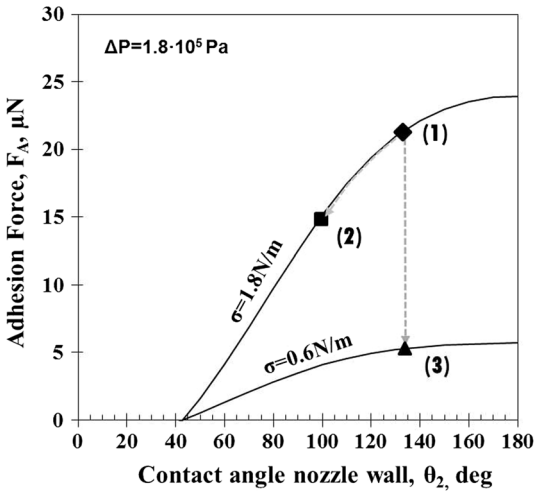

Fig. 8—Model calculation for the relation between the adhesion force, the surface tension of molten steel, and the contact angle at the nozzle wall.

$$a = \left(\frac{6\pi\sigma r_1^2}{K}\right)^{\frac{1}{3}} \quad [25]$$

$$K = \frac{4}{3}\left(\frac{1-\upsilon_1^2}{E_1} + \frac{1-\upsilon_2^2}{E_2}\right)^{-1} \quad [26]$$

where r_1 is the particle radius (m); a is the contact radius; K is the elastic constant (Pa); and υ_i and E_i (i = 1, 2) are the Poisson's ratio and Young's modulus (Pa) of a particle and a surface, respectively.[80] Value 1.4 was chosen by Shi *et al.*[80] to calculate the drag force at the maximum.

An inclusion will be detached when the torque ratio, R_T, becomes larger than unity, meaning that the detachment forces acting on the inclusion are stronger than the adhesion force. The fluid flow conditions next to the wall strongly influence the torque ratio given by Eq. [27]:

$$R_T = \frac{1.4 r_1 F_D + a F_L - r_1 F_B}{a F_A} \quad [27]$$

III. CASE STUDIES

Steel grades that possess an increased tendency to clog are ones containing elements with high affinities for oxygen, sulfur, or nitrogen. Examples of such elements are aluminum, rare earth metals, calcium, or titanium, and these are able to form solid NMIs, such as Al_2O_3 or CaS, in the liquid steel.

Special importance over the years is given to clogging caused during the production of Al-killed steels.[5,12,13,19,20,24,31–33,44,49,58,81–85] In these steels, the solid aluminum oxides formed due to deoxidation already in the liquid steel during tapping and subsequent ladle treatment. Their high contact angle of 137 deg with molten iron is believed to be the reason that these steels have a high risk of clogging the SEN. The adhesion force calculated between a 5-μm-diameter aluminum oxide and an alumina-based refractory wall, according to Eq. [3], is plotted in Point (1) of Figure 8.

A reduction of the adhesion force presented in Point (1) is possible under the assumption that the new nozzle material chosen has a better wettability for liquid steel than the alumina-based refractory used before. It must be stated that refractories with good wettability for liquid steel generally also exhibit a higher reactivity with steel. Nadif *et al.*[3] conclude that it appears to be impossible to find a refractory nozzle material with a low contact angle (below 40 to 60 deg) without a high reactivity.[3,86] As a compromise, a zirconia-based refractory was chosen for this analysis because it has a contact angle of 100 deg. In Point (2) of Figure 8, the reduction of the adhesion force for the alternative nozzle material can be observed.

Another possibility for the reduction of the adhesion force is related to the reduction of the surface tension between steel and the fluid phase inside the cavity. Sasai and Mizukami[34] and Mizoguchi *et al.*[39] suggested a mechanism by which FeO particles could act as a binder for the alumina particles. Lee *et al.*[29] emphasized the importance of the interfacial conditions in contraposition with the bulk conditions. In the interface between steel and the refractory, a local increase of the oxygen concentration may lead to steel reoxidation.

The surface tension between molten steel and a gas or vapor contained in the cavity is considered to be 1.8 N/m. However, the surface tension between molten steel and FeO is approximately 0.6 N/m.[45,87] Therefore, if a liquid bridge is formed, the adhesion force between an aluminum oxide inclusion and an alumina-based nozzle wall is reduced, as shown in Point (3) of Figure 8.

Since the FeO formation on an industrial scale may not be common, this third case should be seen as an approximation for the use of lime-bearing or calcium zirconate nozzle materials mentioned previously. The presence of a liquid bridge reduces the adhesion force in comparison to the gaseous case, and a further reduction in adhesion force would be expected if the solid inclusion becomes liquid or semiliquid.

The force balances proposed in the detachment criteria have been solved for the three cases presented in Figure 8. The properties necessary for the calculations are found in Table III. Since the lift force is small in comparison to the adhesion force the normal ratio given by Eq. [21] could be neglected. The parallel ratio, given by Eq. [23], increases with the change of the friction coefficient from 0.3 (in Case (1) and (2)) to 0.1 (in Case (3)). However, in all calculations, the torque ratio [Eq. 27] is the limiting one. As a result, the minimum velocity needed for detaching an inclusion at the inclusion's center of mass is presented in Figure 9. The reduction of the adhesion force, from Case (1) to Case (3), leads to a decrease in the minimal steel velocity at the wall near the particle location for detaching the particle. To remove a 20 μm alumina inclusion in Case (1), the minimum steel flow velocity next to the wall would be at least 1, 0.8 m/s for Case (2) and 0.4 m/s for

Table III. Material Properties[88]

		Liquid Steel			Nozzle Material				NMI				
Calculated Case	Cavity Fluid	σ (N/m)	ρ (kg/m^3)	ν (m^2/s)	2	θ_2 (Deg)	E_2 (GPa)	ν_2	1	θ_1 (Deg)	E_1 (GPa)	(ν_1)	ρ_1 (kg/m^3)
(1)	gas	1.8	7000	$7.14 \cdot 10^{-7}$	Al_2O_3 based	137	314	0.27	Al_2O_3	137	314	0.27	3950
(2)					ZrO_2 based	100	175	0.27					
(3)	liquid FeO	0.6			Al_2O_3 based	137	314	0.27					

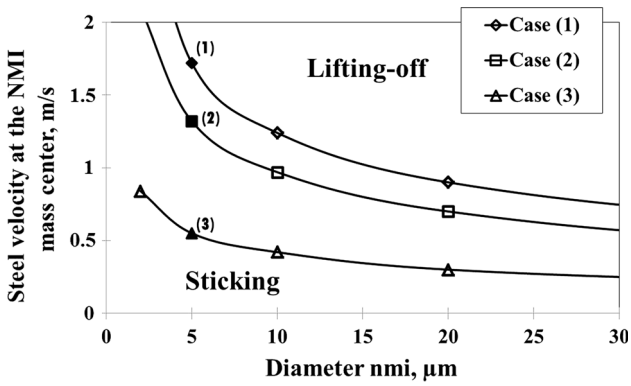

Fig. 9—Relation between the steel velocity and the particle diameter for the detachment criteria according to Eqs. [21], [23], and [27].

Case (3). As the inclusion size increases, it becomes easier for the force of the steel flow to detach the particle.

In industrial practice, the inclusions found in the clogging deposits are in a range of 1 to 10 μm. From Figure 9, the NMIs in this range may need even higher steel velocities in the near-wall region to be removed, which further underscores the importance of understanding fluid flow in the near-wall region. From the previous calculations, the inclusions within the mentioned range would be completely immersed inside the laminar layer (in accordance with our model), and due to the low velocities in the laminar layer, they will not be detached.

Another factor to take into account is the roughness of the wall. The roughness may help to introduce some disturbances in the laminar layer and produce a local fluctuating component of the velocity. In turbulent flow, the instantaneous values of velocity fluctuate about a mean value. This fluctuating component in the turbulent near-wall region may be responsible for a temporary increase or decrease of the steel velocity at the particle's position. As this fluctuation could be of the same magnitude as the average mean velocity, it eventually can lead to a possible detachment depending on the inclusion size and the material-related properties such as contact angle and surface tension. The inclusion detachment may be linked to the formation of unsteady turbulent eddies in the near-wall region.

Over the years, it was stated that hydrodynamic conditions strongly influence the deposition of the inclusions.[4,15] In Section I, it was mentioned that the clogging tendency of NMIs should increase due to the presence of turbulent, as well as dead, areas in the system. The current work gives insight on how the hydrodynamic conditions may influence the detachment of NMIs from the wall. Figure 9 illustrates that in areas of low velocity in the near wall (dead or stagnant zones), the NMIs would not be detached; thus, the clogging tendency would increase. Whereas, turbulent eddies in the near-wall zone may enhance the detachment of NMIs. From the results obtained in Figures 8 and 9, it is apparent that the modification of the refractory wettability proposed previously (from Case (1) to Case (2)) is not enough to cause a radical decrease of the adhesion forces and, therefore, to permit the detachment of inclusions from the nozzle wall. The controlled formation of a liquid phase between the inclusion and the nozzle (Case (3)) improves detachment in comparison to the initial case, suggesting that modifying the solid inclusions so that they become low melting phases at the refractory/steel interface might reduce clogging.

Argon is commonly injected in the SEN with the intention of reducing the adhesion forces between the small inclusions and the nozzle wall. Future research will be focused on the behavior of NMIs when argon is present in the SEN.

IV. CONCLUSIONS

- An inclusion generated from steel deoxidation and further transported to the near-wall region will adhere by forming a cavity bridge against the nozzle wall to reduce its interfacial energy. This inclusion will be subjected to forces related to the material properties and to the fluid flow conditions in the near-wall region. A detachment criterion was presented based on the normal and parallel force balance and on the torque moment of the inclusion. The condition for an inclusion detachment occurs when one of the three force ratios presented (normal, parallel, or torque) is equal to or greater than unity. The torque moment is the limiting ratio in all the calculated cases.
- As a result, the conditions by which the steel flow can detach an inclusion of a specific size at the near-wall area was presented for three cases: (1) alumina inclusion/alumina-based nozzle wall, (2) alumina inclusion/zirconia-based nozzle, and (3) alumina/alumina with a FeO bridge as a binder. It was observed that a reduction of the adhesion force, from Case (1) to Case (3), led to a decrease in the minimal steel flow velocity needed at the near-wall particle position to detach the particle.

- Due to the small size of the inclusions found in the clogging deposits and the low velocities next to the wall either in laminar flow or in the laminar layer of turbulent flow, no detachment will be observed. Conditions for successful detachment were even more critical in stagnant regions. Near-wall turbulences due to the fluctuating component of the velocity could locally and temporarily increase the velocity in the near-wall region, possibly leading to conditions favorable to detach.
- The modification of the refractory wettability proposed previously (from Case (1) to Case (2)) was not enough to cause a radical decrease of the adhesion forces and, therefore, to permit the detachment of inclusions from the nozzle wall. The controlled formation of a liquid phase between the inclusion and the nozzle (Case (3)) showed an improvement compared to the initial case, suggesting that modifying solid inclusions so that they become low melting phases at the refractory/steel interface might be applied as a good clogging countermeasure.

ACKNOWLEDGMENTS

The financial support by K1-Met GmbH is gratefully acknowledged. K1-Met is a member of COMET—Competence Center for Excellent Technologies and is financially supported by the Austrian ministries BMVIT and BMVITJ; the provinces of Upper Austria, Styria, and Tyrol; SFG; and Tiroler Stiftung. COMET is managed by FFG (Austrian research promotion agency).

REFERENCES

1. V. Vermeulen, B. Coletti, B. Blanpain, P. Wollants, and J. Vleugels: *ISIJ Int*., 2002, vol. 42, pp. 1234–40.
2. K.G. Rackers and B.G. Thomas: Iron and Steel Society, Warrendale, PA, 1995, vol. 78, pp. 723–34.
3. M. Nadif, M. Burty, H. Soulard, M. Boher, C. Pusse, J. Lehmann, and F. Meyer: *IISI Study on Clean Steel*, 1st ed., IRSID, Acerlor, France, 2004, pp. 87–135.
4. F.G. Wilson, M.J. Heeson, and J.D.W. Rawson: *Tech. Steel Res*., 1988, pp. 1–5.
5. S.N. Singh: *Metall. Trans*., 1974, vol. 5, pp. 2165–78.
6. S. Ogibayashi: *Taikabutsu Overseas*, 1995, vol. 15, pp. 3–13.
7. B.G. Thomas, A. Dennisov, and H. Bai: *ISS 80th Steelmak. Conf*., 1997, pp. 375–84.
8. B.F. Thomas and H. Bai: *Iron Steel Soc*., 2001, vol. 18, pp. 895–912.
9. E.S. Szekeres: *IV Int. Conf. on Clean Steel,* 1992, pp. 756–76.
10. Y.K. Shin, I.R. Lee, D.S. Kim, S.K. Kim, and K.S. Oh: *Ironmak. Steelmak*., 1988, vol. 15, pp. 143–49.
11. E. Roos, A. Karasev, and P.G. Jönsson: *Steel Res. Int*., 2015, vol. 86, pp. 1279–88.
12. J. Poirier, B. Thillou, M.A. Guiban, and G. Provost: *Steelmak. Conf. Proc*., 1995, pp. 451–56.
13. R. Tuttle, K.D. Peaslee, and J.D. Smith: *AISTech Conf. Proc*., 2002, pp. 1–11.
14. M. Suzuki, Y. Yamaoka, N. Kubo, and M. Suzuki: *ISIJ Int*., 2002, vol. 42, pp. 248–56.
15. S. Dawson: *Ironmak. Steelmak*., 1990, vol. 17, pp. 33–42.
16. H. Bai and B.G. Thomas: *Metall. Mater. Trans. B*, 2001, vol. 32B, pp. 707–22.
17. H. Bai and B.G. Thomas: *83rd Steelmak. Conf. Proc*., 2000, pp. 183–97.
18. K. Sasai and Y. Mizukami: *ISIJ Int*., 1995, vol. 35, pp. 26–33.
19. Y. Fukuda, Y. Ueshima, and S. Mizoguchi: *ISIJ Int*., 1992, vol. 32, pp. 164–68.
20. S. Ramachandran, K.D. Peaslee, and J.D. Smith: *Steelmak. Conf. Proc*., 2001, 729–34.
21. N. Kasai, M. Kawasaki, Y. Hayashi, and H. Kawai: *Taikabutsu Overseas*, 1991, vol. 11, pp. 22–33.
22. H. Shikano, T. Harada, S. Iitisuka, and K. Shin-Ichirou: *Taikabutsu Overseas*, 1991, vol. 11, pp. 10–21.
23. L. Zhang: *J. Iron Steel Res. Int*., 2006, vol. 13, pp. 1–8.
24. S. Liu, S. Niu, M. Liang, C. Li, X. Zuo, L. Zhang, and X. Wang: *AISTech Conf. Proc*., 2007, vol. 10, pp. 1–10.
25. G.T. Moulden and R. Sabol: *Steelmak. Conf. Proc*., 2000, pp. 161–66.
26. V. Brabie: *ISIJ Int*., 1996, vol. 36, pp. 109–12.
27. W. Höller: *Veitsch-Radex Rundschau*, 1998, vol. 2, pp. 13–22.
28. M. Nakamura, T. Yamamura, O. Nomura, R. Nakamura, and E. Iida: *Taikabutsu Overseas*, 1997, vol. 17, pp. 34–40.
29. J. Lee, S. Kim, M. Kang, and Y. Kang: *ECCC Conf. Proc*., 2017, pp. 1–6.
30. J. Szekely and S.T. Dinovo: *Metall. Trans*., 1974, vol. 5, pp. 747–54.
31. G.C. Duderstadt, R.K. Iyengar, and J.M. Matesa: *J. Met*., 1968, vol. 4, pp. 89–94.
32. J.W. Farrell and D.C. Hilty: *Electr. Furn. Conf. Proc*., 1971, pp. 31–46.
33. M. Andersson and O. Wijk: *6th Int. Conf. Refin. Processes*, 1992, pp. 175–209.
34. K. Sasai and Y. Mizukami: *ISIJ Int*., 2001, vol. 41, pp. 1331–39.
35. K. Uemura, M. Takahashi, S. Koyama, and M. Nitta: *ISIJ Int*., 1992, vol. 32, pp. 150–56.
36. E. Kawecka-Cebula, Z. Kalicka, and J. Wypartowicz: *Arch. Metall. Mater*., 2006, vol. 51, pp. 261–68.
37. C.G. Aneziris, C. Schroeder, M. Emmel, G. Schmidt, H.P. Heller, and H. Berek: *Metall. Mater. Trans. B*, 2013, vol. 44B, pp. 954–68.
38. K. Sasai: *ISIJ Int*., 2014, vol. 54, pp. 2780–89.
39. T. Mizoguchi, Y. Ueshima, M. Sugiyama, and K. Mizukami: *ISIJ Int*., 2013, vol. 53, pp. 639–47.
40. Y. Ueshima, T. Mizoguchi, M. Sugiyama, and K. Mizukami: *5th Int. Congr. Sci. Technol. Steelmak.,* Dresden, Germany, 2012.
41. L. Zheng, A. Malfliet, P. Wollants, B. Blanpain, and M. Guo: *ICS Conf. Proc*., 2015, pp. 731–36.
42. L. Zheng, A. Malfliet, P. Wollants, B. Blanpain, and M. Guo: *ISIJ Int*., 2016, vol. 56, pp. 926–35.
43. C. Xuan, A.V. Karasev, P.G. Jönsson, and K. Nakajima: *Steel Res. Int*., 2017, vol. 88, pp. 911–20.
44. J. Poirier, D. Verrelle, B. Thillou, G. Provost, C. Taffin, and P. Tssot: *UNITECR Conf. Proc*., 1991, pp. 226–29.
45. A.W. Cramb and I. Jimbo: *W.O. Philbrook Meml. Symp. Conf. Proc*., 1988, pp. 43–55.
46. P.M. Benson, Q.K. Robinson, and H.K. Part: *Steelmak. Conf. Proc*., 1993, pp. 533–39.
47. E. Lührsen, A. Ott, W. Porbel, J. Piret, R. Ruddlestone, and B. Short: *1st ECCC Conf. Proc*., 1991, pp. 137–57.
48. R. Tsujino, A. Tanaka, A. Imamura, D. Takahashi, and S. Mizoguchi: *ISIJ Int*., 1994, vol. 34, pp. 853–58.
49. T. Nakamura, T. Aoki, H. Okumura, and Y. Kondo: *Taikabutsu Overseas*, 1991, vol. 11, pp. 38–40.
50. K. Oguri, M. Ando, T. Muroi, T. Aoki, and H. Okumura: *UNITCER '93,* 1993, pp. 1119–29.
51. T. Aoki, T. Nakamura, H. Ozeki, and A. Elksnitis: *Steelmak. Conf. Proc*., 1991, pp. 357–60.
52. F. Ohno, T. Muroi, and K. Oguri: *J. Tech. Assoc. Refract*., 2002, vol. 22, pp. 63–66.
53. W. Zhong, W. Li, and X. Zhong: *Adv. Refract. Metall. Ind. II,* 1996, pp. 441–52.
54. N. Tsukamoto, Y. Kurashina, and K. Yanagawa: *Taikabutsu Overseas*, 1995, vol. 15, pp. 43–49.
55. T. Kawamura, S. Niwa, E. Hasebe, and T. Simoda: *UNITCER '93 Conf. Proc*., 1993, pp. 1–13.
56. S. Yokoya, S. Takagi, H. Souma, M. Iguchi, Y. Asako, and S. Hara: *ISIJ Int*., 1998, vol. 38, pp. 1086–92.

57. G. Hackl, G. Nitzl, D. Warrington, A. Westendorp, and R. Bogert: *7th ECCC Conf. Proc.*, 2011, pp. 1–7.
58. A.R. McKague, R. Enger, M.A. Suer, D.J. Wolf, M.D. Garbowsky, and L.E. Reed: *Iron Steelmak.*, 1998, vol. 25.
59. J.J. Vitlip and J.E. Roush: *Steelmak. Conf. Proc.*, 2001, pp. 33–40.
60. C.E. Cicutti, J. Madías, and J.C. González: *Ironmak. Steelmak.*, 1997, vol. 24, pp. 155–59.
61. C. Cicutti, M. Valdez, T. Pérez, R. Ares, R. Panelli, and J. Petroni: *Steelmak. Conf. Proc.*, 2001, pp. 871–82.
62. N. Bannenber: *Steelmak. Conf. Proc.*, 1995, pp. 457–63.
63. G.M. Faulring, J.W. Farrell, and D.C. Hilty: *Contin. Cast. Conf. Proc.*, 1995, vol. 1, pp. 57–66.
64. M.K. Sardar, S. Mukhopadhyay, U.K. Bandopadhyay, and S.K. Dhua: *Steel Res.*, 2007, vol. 78, pp. 136–40.
65. M. Alavanja, R.T. Gass, R.W. Kittridge, and H.T. Tsai: *Steelmak. Conf. Proc.*, 1995, pp. 415–26.
66. J. Hartmüller and S. Ripperger: *F. S.*, 2014, vol. 28, pp. 274–77.
67. G. Lian, C. Thornton, and M.J. Adams: *J. Coll. Interface Sci.*, 1993, vol. 161, pp. 138–47.
68. RA Fisher: *J. Agric. Sci.*, 1926, vol. 16, pp. 492–505.
69. D. Rossetti and S.J.R. Simons: *Powder Technol.*, 2003, vol. 130, pp. 49–55.
70. A. Gladkyy and R. Schwarze: *Granul. Matter*, 2014, vol. 16, pp. 911–20.
71. H.P. Zhu, Z.Y. Zhou, R.Y. Yang, and A.B. Yu: *Chem. Eng. Sci.*, 2007, vol. 62, pp. 3378–96.
72. M.A. Fortes: *Can. J. Chem.*, 1982, vol. 60, pp. 2889–95.
73. S. Seetharaman: *Fundamentals of Metallurgy*, 1st ed., CRC Press, New York, 2005.
74. J.N. Israelachvili: *Intermolecular and Surface Forces*, 2nd ed., Academic Press, New York, 2011.
75. R Clift, JR Grace, and ME Weber: *Blubbles, Drops, and Particles*, 1st ed., Dover Publications, Inc., New York, 1978.
76. J.W. Cleaver and B. Yates: *J. Coll. Interface Sci.*, 1973, vol. 44, pp. 464–74.
77. R.J. Garde and K.G. Ranga Raju: 3rd ed., Taylor & Francis, 2000.
78. D. Leighton and A. Acrivos: *Z. Angew. Math. Phys.*, 1985, vol. 36, pp. 174–78.
79. T. Hibiki and M. Ishii: *Chem. Eng. Sci.*, 2007, vol. 62, pp. 6457–74.
80. L. Shi and D.J. Bayless: *Powder Technol.*, 2007, vol. 173, pp. 29–37.
81. C. Toulouse, A. Pack, A. Ender, and S. Petry: *7th ECCC Conf. Proc.*, 2011, pp. 1–8.
82. K. Asano, A. Ishii, and K. Kasai: *UNITECR Conf. Proc.*, 1991, pp. 229–32.
83. L. Luyckx and S. Robinson: *McLean Symp. Proc.*, 1998, pp. 111–26.
84. R. Rastogi and A.W. Cramb: *Steelmak. Conf. Proc.*, 2001, pp. 789–829.
85. D. Janis, A. Karasev, R. Inoue, and P.G. Jönsson: *Steel Res. Int.*, 2015, vol. 86, pp. 1271–78.
86. N. Eustathopoulos and B. Drevet: *J. Phys. III*, 1994, vol. 4, p. 1985.
87. K. Ogino, S. Hara, T. Miwa, and S. Kimoto: *Trans. ISIJ*, 1984, vol. 24, pp. 522–31.
88. D. Munz and T. Fett: *Ceramics: Mechanical Properties, Failure Behaviour Materials Selection*, 2nd ed., Springer, New York, 2013.